JOURNAL OF GEOPHYSICAL RESEARCH, VOL. 113, C09009, doi:10.1029/2006JC003864, 2008

Click Here for Full Article

Temperature finestructure in the Indonesian Seas

Amy Ffield[1] and Robin Robertson[2]

Received 4 August 2006; revised 12 December 2007; accepted 30 May 2008; published 4 September 2008.

[1] Twenty-one years of eXpendable BathyThermograph temperature profile data are used to examine the spatial and temporal variability in finestructure throughout the Indonesian Seas region. Finestructure is the variation of vertical properties on scales from several meter to tens of meter thickness, and is associated, for example, with internal wave activity, an evolving system that can be a precursor to turbulent vertical mixing. As might be expected, on average, the highest temperature finestructure values are observed within 5 km of the shelf-slope boundary, especially within straits, and the lowest values at distances greater than 35 km. However, the long-period time variability in the temperature finestructure reveals significant, unexpected, depth-dependent monsoonal and interannual modulations. In the upper 100 m, there is a 63% enhancement in the temperature finestructure during the windy Southeast Monsoon months of June, July, and August (in particular during La Niña years), relative to the low-wind intermonsoon months of September, October, and November (in particular during El Niño years). Below 100 m, the monsoon influence is much reduced, but surprisingly significant interannual temperature finestructure variability is observed down to 600-m depth with a signal opposite to that in the upper layer of the ocean: a 6-month lagged 13% enhancement associated with El Niño relative to La Niña time periods between 100- and 600-m depths. These results provide a background framework in which to interpret modeling and observational vertical mixing studies in the Indonesian Seas region.

Citation: Ffield, A., and R. Robertson (2008), Temperature finestructure in the Indonesian Seas, *J. Geophys. Res.*, *113*, C09009, doi:10.1029/2006JC003864.

1. Introduction

[2] The Indonesian throughflow carries thermocline waters from the western Pacific Ocean through the many seas and straits of the Indonesian Seas into the Indian Ocean providing the sole equatorial link in the global thermohaline circulation [*Gordon*, 2005; *Susanto and Gordon*, 2005; *Molcard et al.*, 1996, 2001; *Murray and Arief*, 1988; *van Aken et al.*, 1988] (Figure 1). However, the incoming stratified Pacific thermocline waters are altered by vertical mixing, such that the distinctive salinity maximums originating from the North Pacific (salinity of 34.8 at 100 m) and the South Pacific (salinity of 35.4 at 150 m) disappear while within the Indonesian Seas. Consequently, by the time the throughflow waters leave the Indonesian Seas to enter the Indian Ocean, they carry homogeneous salinities (34.6) throughout the upper thermocline [*Ffield and Gordon*, 1992; *Hautala et al.*, 1996]. Vertical mixing within the Indonesian Seas also draws heat and freshwater from the equatorial sea surface down into the Indonesian thermocline contributing to the modification of the Pacific Ocean thermocline waters and increasing the throughflow's buoyancy before it enters the Indian Ocean [*Ffield and Gordon*, 1996]. Therefore quantifying vertical mixing, and its temporal and spatial variability, is necessary in order to assess its impact on the ocean, ocean-atmosphere boundary, and ultimately climate. However, not only are the products of the vertical mixing of interest, but also the driving forces of the mixing; for example, when and where internal waves are generated and propagate affecting, (1) ocean hydrodynamics and physical structures by large amplitude displacement and velocity fluctuations, and (2) ocean acoustics through temperature anomalies that modify the low-frequency sound channel and through generated turbulence that scatters high-frequency sound.

[3] As of yet, a consistent overall description and quantification of the internal wave field and the mixing mechanisms and rates in the Indonesian Seas has not been attained, whether by observations or by models. In the upper thermocline of the Indonesian Seas, the basin-averaged, time-averaged estimates of vertical mixing inferred from stratification changes in the water column are high, on order of 1×10^{-4} m^2 s^{-1} [*Hautala et al.*, 1996; *Ffield and Gordon*, 1996]. For the southern Makassar Strait region in the Indonesian Seas, a 2-d nonhydrostatic model produces tidally generated internal waves that induce vertical mixing as high as 6×10^{-3} m^2 s^{-1} [*Hatayama*, 2004]. Fortnightly tidal signatures are observed in temperature and salinity data in the Indonesian Seas [*Sprintall et al.*, 2003], and several studies have also considered tidal enhancement to vertical

[1]Earth and Space Research, Upper Grandview, New York, USA.
[2]School of Physical, Environmental, and Mathematical Sciences, Australian Defence Force Academy, Canberra, ACT, Australia.

Copyright 2008 by the American Geophysical Union.
0148-0227/08/2006JC003864$09.00

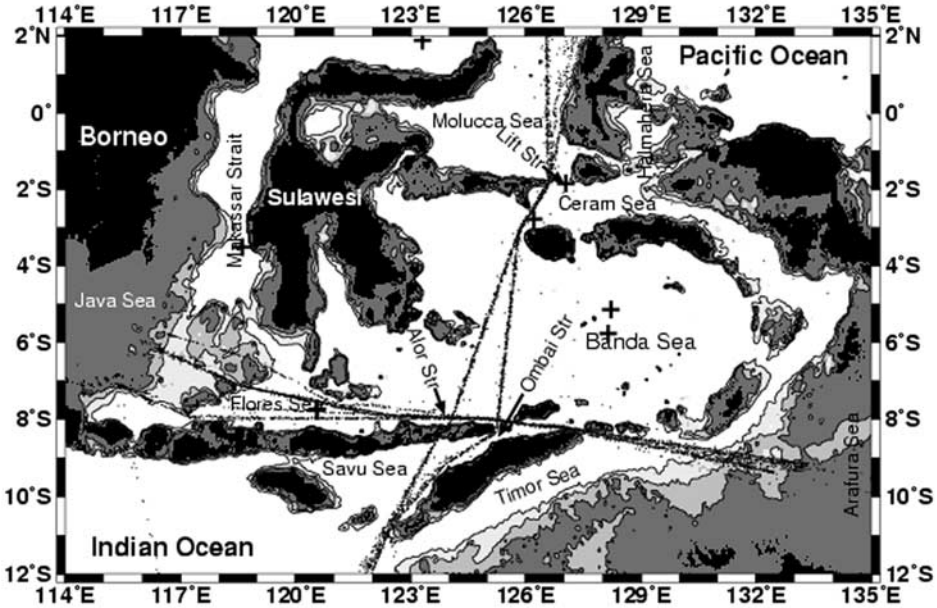

Figure 1. Map of the Indonesian Seas region. The locations of the 8398 XBT profiles (tiny circles) and the eight CTD yo-yo stations (large crosses) are shown. Land is black. Bathymetry is grey shaded and contoured for 100-, 350-, and 750-m depths and is white for depths greater than 750 m.

mixing in the Indonesian Seas by using models [*Hatayama et al.*, 1996; *Murtugudde et al.*, 1998; *Schiller et al.*, 1998] and by identification of tidal mixing signatures in data [*Ffield and Gordon*, 1996]. However, the only direct assessment of vertical mixing in the Indonesian Seas, a 2-week microstructure experiment at a site in the Banda Sea, distant from direct topographic influence and toward the end of a low-wind intermonsoon period, did not reveal enhanced vertical mixing rates, but just typical "open ocean" values with a cruise mean diapycnal diffusivity of $9.2 \pm 0.55 \times 10^{-6}$ m^2 s^{-1} between 20- and 300-m depth [*Alford and Gregg*, 1999]. The isopycnal displacements of the 519 profiles from that October–November 1998 experiment were found to have diurnal and semidiurnal tidal signatures of only 5 to 15 m RMS [*Alford and Gregg*, 1999], whereas in August 1993 and February 1994, during the windy Southeast and Northwest monsoons, peak-to-peak isopycnal displacements were observed to be 55 m during a 12-hour yo-yo station in a different location in the Banda Sea [*Ffield and Gordon*, 1996]. Considered all together, these various results point toward a discontinuity between single mechanism/location/time studies versus averaged-effect studies. But, the microstructure measurements did identify three cycles of discrete energetic mixing by a near-inertial wave during the 14-day experiment [*Alford and Gregg*, 2001]. The inferred generation of the near-inertial wave coincides with the end of the windy Southeast Monsoon around 20 days earlier. Estimating the wind-generated near-inertial wave mixing (dominated by the monsoon variability), the predicted annual-average mixing halves the apparent discontinuity between the microstructure measurements [*Alford and Gregg*, 1999] and the basin-averaged, time-averaged estimates of vertical mixing [*Hautala et al.*, 1996; *Ffield and Gordon*, 1996]. Consequently, in the Indonesian Seas region vertical mixing through breaking internal waves is likely a combination of both the wind and the tides [*Alford and Gregg*, 2001].

[4] In order to begin to address the apparent discontinuity in vertical mixing studies, 21-years of eXpendable Bathy-Thermograph (XBT) data in the Indonesians Seas region are used in this study to quantify the temperature finestructure, defined as vertical variations from several meters to tens of meters thickness, as a function of location, depth, and time. Finestructure is associated, for example, with internal wave activity, an evolving system that can be a precursor to turbulent vertical mixing. In an earlier study the same XBT data were used to assess larger-scale temperature variance along horizontal depth surfaces revealing that 70% of the thermocline temperature interannual variability can be accounted for by Kelvin and Rossby waves generated by remote zonal winds along the equator of the Indian and Pacific Oceans, and that large temperature variability is associated with areas where the thermocline vertical temperature gradient is strongest and near to shelf breaks [*Wijffels and Meyers*, 2004]. In this study, with an approach that focuses on the smaller-scale vertical variations, the XBT results reveal large-scale geographical and temporal variability in the finestructure of the Indonesian thermocline, providing a qualitative spatial and temporal background framework in which observational and modeling vertical mixing studies can be interpreted, possibly alleviating the apparent discontinuity in results that may actually be due to real spatial and temporal variability.

2. Data

[5] To motivate and provide context for the XBT analysis of the paper, first, temperature and salinity profile data from Conductivity-Temperature-Depth (CTD) measurements obtained during the joint Indonesian and U.S. "ARLINDO

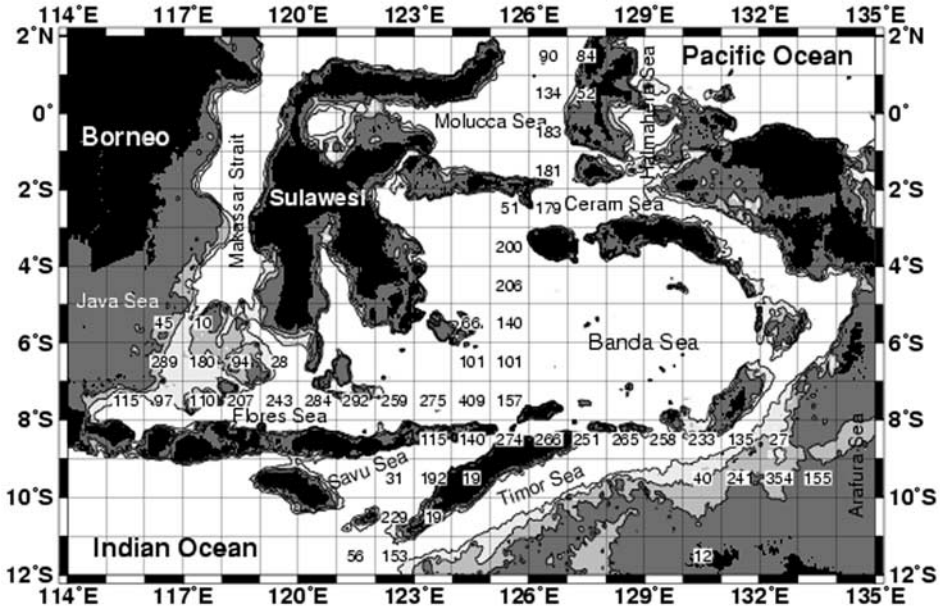

Figure 2. The numbers of XBT profiles in each one-degree square are shown on the map revealing the geographic density in the Indonesian Seas region. Only squares with more than 7 profiles are shown.

Mixing'' cruises are examined. The first cruise was during the southeast monsoon in August–September 1993, and the second cruise was during northwest monsoon in January–February 1994. The CTD data set includes eight yo-yo stations, with four to six CTD casts carried out at the same location within a 12-hour time period during productivity experiments. The yo-yo stations give an indication of the hourly and semi-diurnal variability in the Indonesian thermocline. The CTD temperature values have an initial accuracy of ±0.001°C. In the text the pressure (db) values from the CTD yo-yo stations are referred to as depth (m) values for convenience.

[6] The primary analysis of the paper uses temperature profile data from free-falling XBT probes. The majority of the XBT probes were deployed as part of the upper ocean observing system network along commercial shipping lines by volunteer observers (Figure 1). The data set was obtained from CSIRO in Australia [*Wijffels and Meyers*, 2004]. The XBT shipping lines within the Indonesian Seas region are designated PX2 (the west–east line within a few degrees of 8°S) and IX22 (the north–south line within a few degrees of 126°E) and are generally traversed monthly. All XBT data within the 114°E to 135°E and 12°S to 2°N region are used, composing a total of 8398 temperature profiles, and are henceforth referred to as the ''Indonesian Seas region''. The numbers of XBT profiles in each one-degree square are shown by a map view (Figure 2) to indicate the geographic XBT data density, and the number of XBT profiles in each year in a histogram format (Figure 3) to indicate the overall temporal data density. The data from 1985 to 2006 are used for the time series analyses (21-years). The small number of earlier profiles is also included in the analyses, but, for practicality, the data set is referred to as 21-years long. The XBT profiles initially reached to 460 m nominal depths with 2 m vertical resolution, then in mid-1986 they changed to 760 m nominal depths. The XBT temperature values have

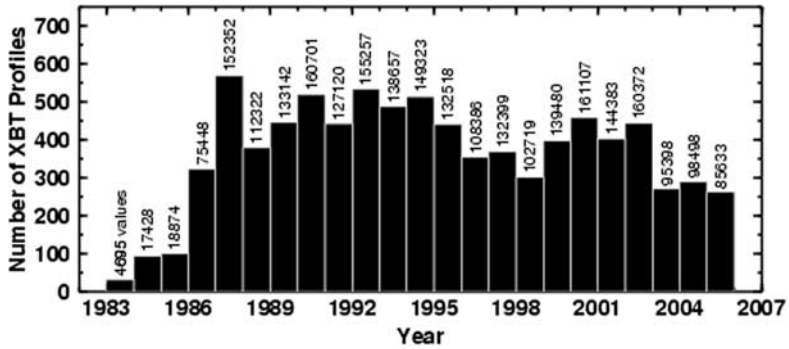

Figure 3. The number of XBT profiles in each year shows the temporal data density in the Indonesian Seas region. As each XBT profile has 2-m-depth resolution, from the sea surface down to 460- or 760-m nominal depths, the number of values is shown over each histogram bar to show the total number of observations.

Table 1. The CTD Yo-Yo Stations With the Longitudes, Latitudes, Dates, Number of Profiles, 25°C Isotherm Peak-to-Peak Heaving (m), 20°C Isotherm Peak-to-Peak Heaving (m), and Age of the Moon (Days Since New Moon)

Yo-Yo Station	Longitudes	Latitudes	Middate	Profiles	25°C Peak-Peak (m)	20°C Peak-Peak (m)	Age (days)
Ceram93	126.2	−2.8	8/24/93	4	42	73	6
Banda93	128.1	−5.8	8/30/93	4	18	22	12
Flores93	120.6	−7.7	9/08/93	4	15	11	21
Flores	120.6	−7.8	1/29/94	5	19	16	17
Banda	128.2	−5.2	2/08/94	4	27	31	27
Lifamatola	127.0	−1.9	2/14/94	5	63	33	3
Sulawesi	123.3	1.9	2/20/94	5	36	30	9
Makassar	118.6	−3.5	2/23/94	6	15	13	12

an accuracy of ±0.1°C, considerably less than the accuracy of the CTD temperature values.

3. Motivation

[7] Temperature and salinity profiles from CTD yo-yo stations reveal the rich complexity of the Indonesian thermocline (Table 1). As there were four to six CTD casts during each 12-hour yo-yo station, the resulting 2 to 3-hour time-resolution at a single location is useful to examine before analyzing the lower accuracy and more widely time and space distributed XBT data set. Three yo-yo stations adjacent to the XBT transects are examined in detail.

[8] At the Lifamatola Strait yo-yo station (127.0°E, 1.9°S), instead of smoothly varying properties with depth, each CTD cast displays considerable temperature and salinity structure with wiggle and step features at 1 to 50 m vertical scales (Figures 4a and 4b). In addition, the five casts reveal significant profile-to-profile time variability over 12 hours with almost none of the smaller-scale temperature and salinity features persisting from cast-to-cast. The stability of the water column is very high in the Lifamatola Strait (and throughout the Indonesian Seas region) because of the large vertical temperature gradient in the upper thermocline, with 20°C temperature change over 300-m depth (0.067°C/m). Yet the vertical movement of the thermocline is also quite high despite the far offshore location. Larger-scale time variability over the 12 hours is revealed by the 20°C isotherm: it begins at 113-m depth, plunges 33 m- to 146-m depth, and then rebounds back to 113-m depth (Figure 4c, squares).

[9] The other CTD yo-yo stations also reveal highly structured thermoclines, and when compared to each other they hint to possible regional differences. Similar to the Lifamatola Strait to the north–east, at the Ceram Sea yo-yo station (126.2°E, 2.8°S) the 20°C isotherm starts at 138-m depth, rises 73- to 65-m depth, and then drops back 56- to 121-m depth over 12 hours (Figure 5c, squares). While, the Ceram Sea smaller-scale temperature and salinity features persist over a short two-hour time period (middle three casts), they do not over the 12-hour time period (Figures 5a and 5b) as with the Lifamatola Strait station. However, at the Flores Sea yo-yo station (120.6°E, 7.8°S), there is considerably less profile-to-profile variability than in the Lifamatola Strait or the Ceram Sea with clear persistence of the smaller-scale temperature and salinity features over the course of the 12 hours (Figures 6a and 6b). The Flores Sea 20°C isotherm starts at 138-m depth, rises 16- to 122-m depth, and then drops 13 m to 135 m (Figure 6c, squares). The shallower 25°C isotherms also reveal a reduced Flores Sea 12-hour time variability with 19 m peak-to-peak heaving, in contrast to the larger Lifamatola Strait 63 m peak-to-peak heaving and Ceram Sea 42 m peak-to-peak heaving. For completeness, the temperature, salinity, and pressure values from the Lifamatola Strait, Ceram Sea, and Flores Sea CTD yo-yo stations are used to calculate buoyancy

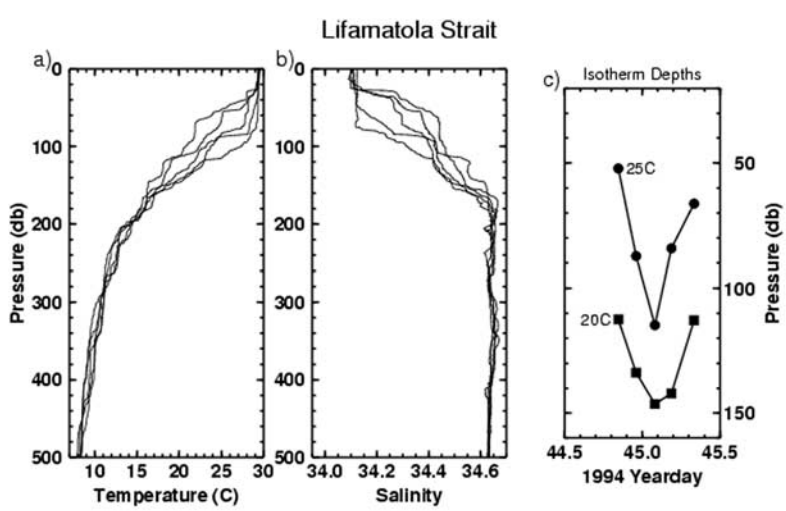

Figure 4. The (a) temperature profiles, (b) salinity profiles, and (c) 20°C (squares) and 25°C (circles) isotherm depth (actually pressure) time series for the CTD yo-yo station obtained over 13 and 14 February 1994 in the Lifamatola Strait (crosses mark the station locations at 127.0°E, 1.9°S in Figure 1).

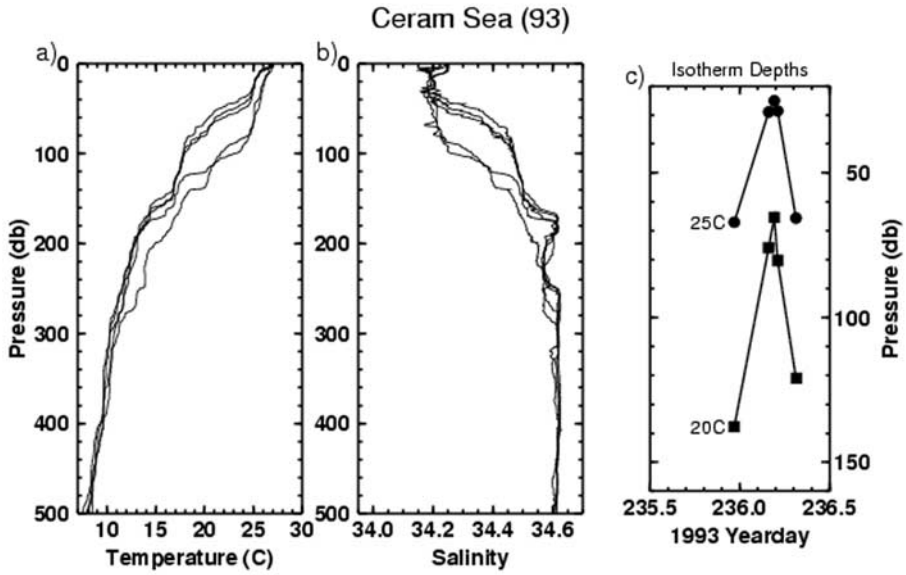

Figure 5. The (a) temperature profiles, (b) salinity profiles, and (c) 20°C (squares) and 25°C (circles) isotherm depth (actually pressure) time series for the CTD yo-yo station obtained over 23 and 24 August 1993 in the Ceram Sea (crosses mark the station locations at 126.1°E, 2.8°S in Figure 1).

frequency values, indicating that the buoyancy frequency is largest, and therefore the water column most stable, near 100 m (Figure 7). In general, the CTD yo-yo stations indicate (1) significant internal wave activity in the region (more so in the Lifamatola Strait and the Ceram Sea), (2) significant fine-scale temperature and salinity structure, a possible precursor to turbulence and mixing, (3) possible spatial variability between the sites, and (4) possible semi-diurnal/diurnal forcing (the isotherm heaving is consistent with 12/24-hour cycles).

[10] While temperature and salinity profiles are typically used to quantify large-scale processes, the profiles also can be used to quantify small-scale processes. For example, observations of density inversions and internal wave vertical strain in temperature and salinity profile data can be used to estimate diapycnal mixing [*Kunze et al.*, 2006; *Polzin et al.*, 1995; *Finnigan et al.*, 2002; *Wijesekera and Dillon*, 1991]. However, the variability in the upper Indonesian thermocline is so large that even the sampling resolution and duration of the CTD yo-yo stations is not adequate to estimate the requisite time-mean density profile needed for those types of calculations. For the XBT data the sampling limitations are much more severe, as there are no salinity measurements, and only about a single temperature profile

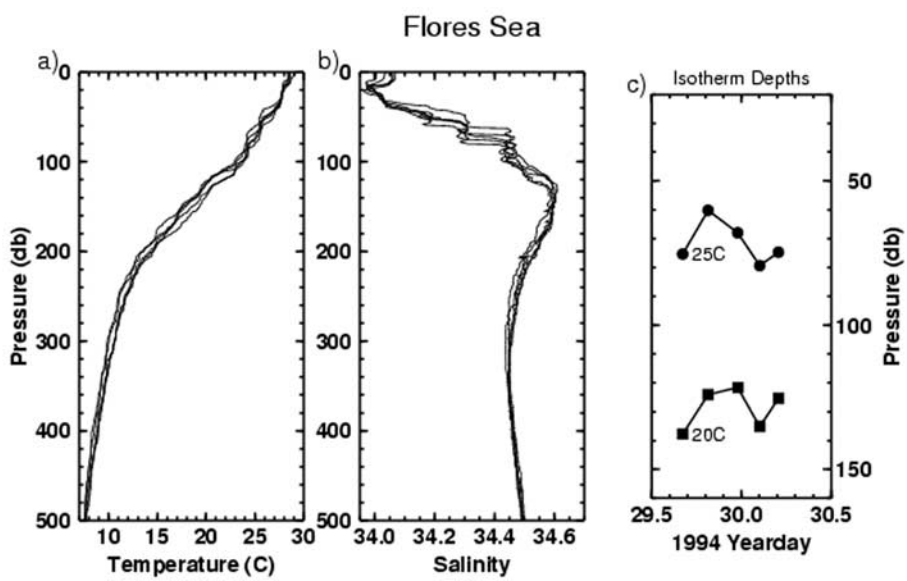

Figure 6. The (a) temperature profiles, (b) salinity profiles, and (c) 20°C (squares) and 25°C (circles) isotherm depth (actually pressure) time series for the CTD yo-yo station obtained over 29 and 30 January 1994 in the Flores Sea (crosses mark the station locations at 120.5°E, 7.8°S in Figure 1).

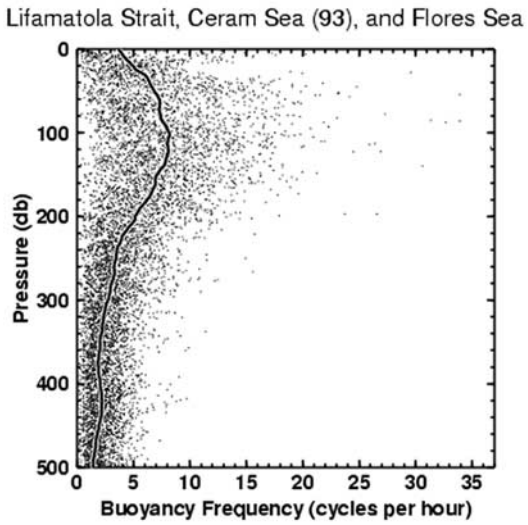

Figure 7. The buoyancy frequency values (dots) and 2-m averages (line) for the Lifamatola Strait, Ceram Sea (93), and Flores Sea CTD yo-yo station temperature and salinity observations.

monthly within a one-degree segment of a shipping lane. (These limitations are in addition to the already noted much reduced XBT temperature accuracy of ±0.1°C, relative to the CTD temperature accuracy of ±0.001°C.) To illustrate the data sampling limitations, the Ceram Sea CTD yo-yo station is used. By averaging the five temperature profiles from the 12-hour yo-yo station, a fairly reasonable time-mean profile seems to be obtained, with the 20°C mean isotherm at 94 m (Figure 8b, star). However, if only the first and last profiles were available, then the 20°C mean isotherm would seem to be at 122 m, and if only the middle three profiles were available, then the 10°C mean isotherm would seem to be a 71 m. It is highly likely that additional profiles outside these observed 12-hours would further change the time-mean profile estimate as there is also significant diurnal and fortnightly variability in the region. This 51-m sensitivity, over just 12-hours, demonstrates that XBT profiles obtained monthly cannot be averaged to estimate a unaliased time-mean for use in quantifying small-scale processes. While studies have also used various mathematical fits to estimate the required time-mean profiles, this as well cannot be applied in the upper Indonesian thermocline. For example, the 5-term polynomial fit by least squares for each temperature profile of the Ceram Sea CTD yo-yo station results in completely different "mean" profiles over the 12-hours with the 20°C "mean" isotherms ranging from 70 to 133 m, a 63 m spread (Figure 8c, circles). In no way is this a defect of the mathematical fit, as without additional data spanning across the semi-diurnal, diurnal, and fortnightly tidal time-periods, the background mean temperature profile in the Indonesian Seas cannot be ascertained from a single profile. In addition, tests reveal (not shown) that polynomial fits generically applied across the entire Indonesian Seas region are systematically skewed in different ways, varying by both geographic location and season, and by the choice of profile segment-length. While those errors might be small, without definitive small-scale information in this region for comparison, this would introduce an unquantifiable and potentially unacceptable aliasing into the study, in particular, because the focus is on assessing the large-scale geographical and temporal differences in the finestructure. For these reasons, the

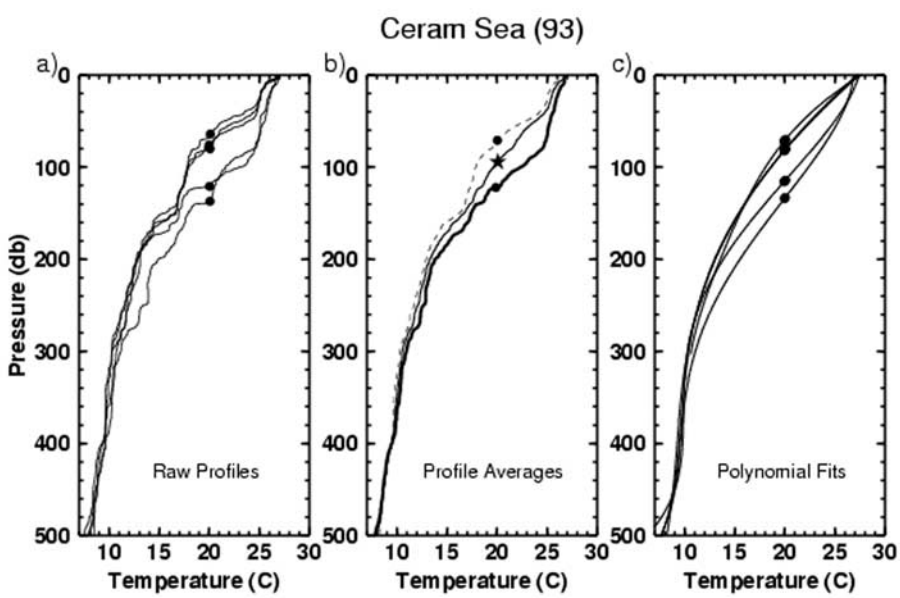

Figure 8. The (a) temperature profiles, (b) temperature profile averages, and (c) estimated "time-mean" temperature profiles (5-term polynomial fit by least squares for each temperature profile) for the CTD yo-yo station obtained over 23 and 24 August 1993 in the Ceram Sea. In Figure 8b, the thin line is the average of all five temperature profiles; the thick line is the average of the first and last profiles which is when the thermocline is deepest; and the dashed line is the average of the three middle profiles which is when the thermocline is shallowest. The solid circles and the star indicate the depth of the 20°C isotherm.

XBT temperature profiles are analyzed in the most simple and strait-forward way, purely quantifying what the eye observes in the temperature profiles, and in this way the results are not compromised by imperfect estimates needed for more complicated calculations.

[11] Henceforth, the XBT data are analyzed instead of the CTD data in order to capitalize on the much larger data set. The possible energy sources and dynamics responsible for the finestructure are not addressed; instead general large-scale location and temporal trends characterizing the fine-scale temperature variability in the Indonesians Seas are sought in order to ascertain an overall representation of the region.

4. Method

[12] In order to characterize the temperature finestructure in the Indonesian Seas, the analysis method in this study focuses on the advantages of the XBT data: good vertical sampling: every 2 m from the sea surface to ~760 m; reasonably accurate temperatures: ±0.1°C, which are sufficient in the Indonesian Seas region because of the large vertical temperature gradients; and excellent large-scale spatial and temporal data coverage: 8398 profiles along two transects over 21-years. The primary disadvantage of the XBT data is the infrequent sampling at a single location: on order of one profile, once a month, in a one-degree square. To overcome this shortcoming, considerable spatial and temporal averaging of the results is used.

[13] The variability in each individual XBT temperature profile is characterized only at 2 to 10 m (finestructure) vertical scales, in order to avoid any contamination by the larger 100 m vertical scale changes associated with seasonal and interannual thermocline stratification variability. The finestructure represents irreversible structures because of recent mixing events [e.g., *Desaubies and Gregg*, 1981], transient vertical displacements due to straining by the internal wave field which ultimately can result in mixing [*Kunze et al.*, 2006], and water mass intrusions/interleaving that in the Indonesian Seas are quickly incorporated (i.e., mixed) into the water column [*Ilahude and Gordon*, 1996; *Hautala et al.*, 1996]. It is therefore reasonable to postulate that elevated levels of variability at the 2 to 10 m vertical scales are ultimately associated with elevated levels of mixing. Regardless, the finestructure itself is a defining characteristic of the Indonesian Seas temperature profiles, and it synthesizes the full range of oceanographic conditions and smaller-scale responses to those oceanographic conditions. Therefore the goal is to identify, as best possible, how the finestructure varies geographically and temporally in the Indonesian Seas region. Specifically, an XBT temperature profile is smoothed by a 10 m running mean and then re-sampled by temperature to every 0.1°C. At each 2 m level in the raw XBT temperature profile, the magnitude of the vertical distance (in meters) between the depths of the raw temperature and corresponding temperature in the smoothed profile is determined. In this way temperature structure at vertical scales between 2 and 10 m are characterized by a vertical distance in meters; for convenience the magnitude of these vertical distances are called "finestructure" henceforth in this study. (This method is not that dissimilar from a Thorpe scale analysis [*Dillon*, 1982], but the reduced temperature accuracy of the XBT measurements prevents most inversions from being identified within the profiles as needed in a Thorpe scale analysis.) In using this finestructure method, any discontinuity from a smoothly varying profile is detected, therefore at the boundary between the base of a surface mixed layer and the more stratified deeper thermocline, a high value of finestructure results; this is perfectly acceptable in terms of the goals of this study as the temperature discontinuity at the base of the mixed layer is indeed an indicator of either active or remnant mixing processes. In addition, the Indonesian Seas temperature (and salinity) profiles often reveal the absence of a mixed layer, as well as the obvious dominance of internal wave processes all the way to the sea surface (e.g., Figures 5, 6, and 8); therefore it is desirable to include the entire depth-range of the XBT profiles in the analysis.

[14] Two examples of the calculation reveal subtle, but quantifiable, differences in temperature finestructure. A temperature profile from near the Ombai Strait reveals various step structures and wiggles (Figure 9a). The associated finestructure profile reveals corresponding features; for example, the temperature step from 260 to 300 m in the temperature profile (Figure 9a) is evident as large spikes in the finestructure profile at 260 and 300 m (Figure 9b). In contrast, a temperature profile from the Flores Sea seems relatively quiescent by eye, with fewer wiggles and step features (Figure 9d), and indeed it does have correspondingly reduced finestructure profile values (Figure 9e). To most simply characterize the finestructure in the thermocline, the finestructure results are averaged between 100 and 300 m. In agreement with the visual assessment of the two profiles, the Ombai Strait finestructure average is large, 3.6 m, versus the much smaller 1.0 m finestructure average for the relatively quiescent Flores Sea profile. This reveals that the small-scale vertical variability in the profiles can be reasonably quantified by this method.

[15] Histograms of the calculation results for the two examples fully characterize the spread in the finestructure values, revealing that both locations are dominated by values less than 5 m. (The distributions are one-sided as the magnitudes of the values are used as noted above.) However, the "jagged" Ombai Strait profile only has 60.8% (Figure 9c) of finestructure values less than 5 m, whereas the more quiescent Flores Sea profile has 74.3% (Figure 9f) of finestructure values less than 5 m, indicative of its smoother temperature profile (Figure 9d). In addition, the Ombai Strait therefore, not only has a greater percentage of larger magnitude finestructure values, but also has the largest magnitudes as illustrated by the right-hand-side tail of the distribution (Figure 9c, down to 0.2% of values between 35 to 40 m) in comparison to the Flores Sea (Figure 9f, down to 0.2% of values between 25 to 30 m). The larger spread in the right-hand-side tail of the Ombai Strait histogram (Figure 9c) is the quantification of its jagged temperature profile, and these high-magnitude "outliers" are very much part of the signal of interest reflecting the step structures and wiggles in its temperature profile (Figure 9a). The simple average of the finestructure values, which is influenced by these important outliers, most easily summarizes the data for this study, although only the unwieldy histograms can fully characterize the distribution

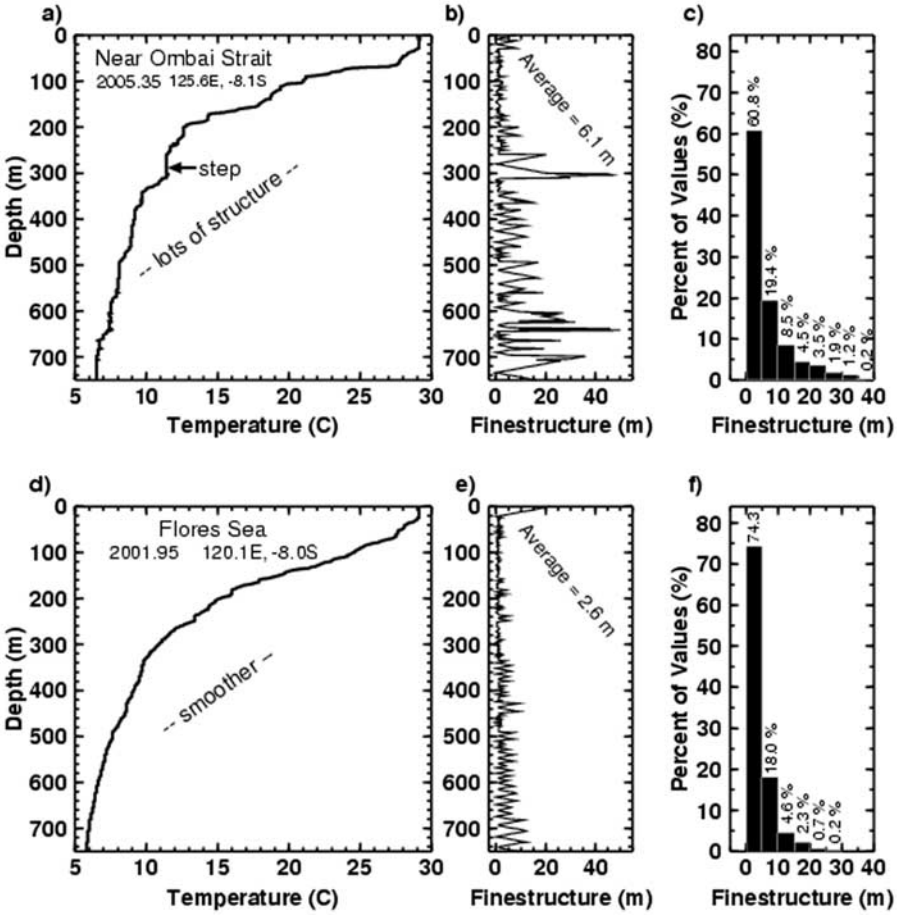

Figure 9. (a, d) Example temperature profiles and their (b, e) corresponding finestructure profiles and (c, f) histograms plots for near the Ombai Strait and in the Flores Sea. These two examples were chosen to focus on midthermocline differences. Near Ombai Strait the (b) finestructure is generally higher because of more vertical temperature structure at 2 to 10 m scales, in contrast to the Flores Sea (e) finestructure because of a comparatively smooth temperature profile at 2 to 10 m scales. The finestructure averages indicated in Figures 8b and 8e are the averages for 0- to 760-m depths. For comparison purposes the finestructure averages for 100- to 300-m depths are (b) 3.6 m and (e) 1.0 m. The histograms of the finestructure show that while both locations are dominated by finestructure values less than 5 m, the (c) Ombai Strait has the largest values and a greater number of larger values in general in comparison to the (f) Flores Sea. (The 10-m smoothing of the profiles used in the finestructure calculation is not shown in Figures 8a and 8d as they would look nearly identical to the raw profiles at these 0–750-m plot scales.)

and reliability of the results with sufficient emphasis on the higher values.

[16] The average of all the finestructure calculation results from within the Indonesian Seas region reveals a profile with minimum finestructure near 200 m and larger finestructure values above 100 m and below 200 m (Figure 10, circles, "mean"). The mean finestructure profile is fairly similar to the mirror image of the buoyancy frequency profile that is typically observed in the Indonesian Seas region (e.g., Figure 7). This is to be expected because vertical displacements are inhibited near the buoyancy frequency maximum relative to the rest of the profile. (The deviations from the "expected" finestructure profile are of considerable interest, but without corresponding salinity measurements, that assessment cannot be made, or even adequately estimated.) The large number of calculated finestructure values (2,450,493) enables the mode, median, mean, central 50% of values, and central 75% to be well-determined as a function of depth for the Indonesian Seas region (Figure 10). As noted for the two example profiles (Figures 9c and 9f), the results are not symmetric on either side of the mean, with most of the values tending toward zero: the histogram for the entire Indonesian Seas region reveals that most of the values (78.7%) are less than 5 m, with 10.7% of all values equaling zero indicating a smoothly-varying temperature profiles (Figure 11). The large magnitude values (right-hand-side tails) are the most-distinguishing features of the distributions (e.g., 87.5% whiskers, "]", on Figure 10), and of particular interest as they are possible indicators of infrequent but energetic phenomena/events. However, as all the histograms reveal a consistently smooth drop-off in the distributions (Figures 9c, 9f, and 11), a simple average of the finestructure

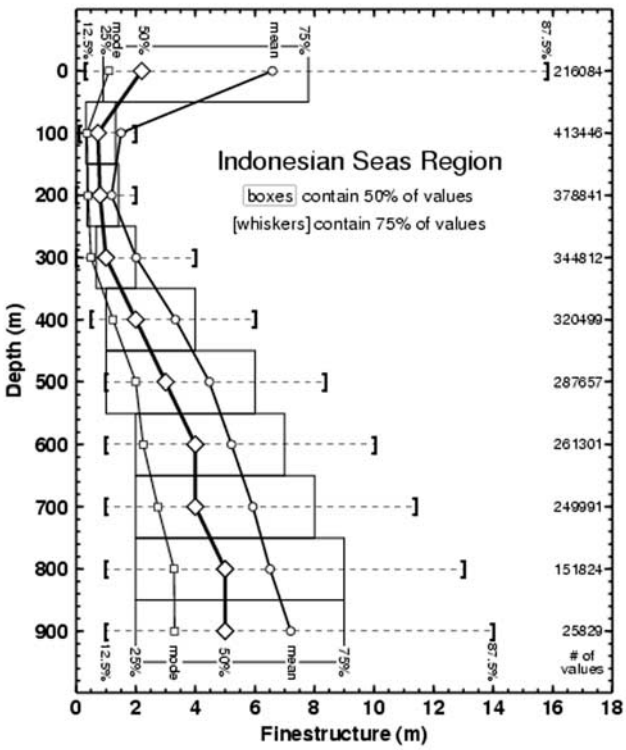

Figure 10. The mean (circles) finestructure profile for the 114°E to 135°E and 12°S to 2°N region (8398 profiles), and the mode (squares), median (diamond), middle 50% of values (boxes), and middle 75% of values (whiskers) to indicate the central spread of the finestructure values. The number of observations per depth interval is shown on the right side of the plot. The general shape of the profile is similar to the mirror image of the buoyancy frequency profile with minimum finestructure and maximum buoyancy frequency near 100 m and larger finestructure and smaller buoyancy frequency above and below 100 m.

results reliably, and most easily, characterizes the data results for this study.

5. Results

5.1. Geographic Variability

[17] In order to first gain a straightforward geographical perspective of the average differences in finestructure within the Indonesians Seas region, three depth intervals are averaged, heavily smoothed horizontally by a 3° × 3° filter, and plotted by map-view (Figure 12). In the upper 10 to 100 m (Figure 12a), the finestructure is strongly influenced by monsoon wind variability, with the largest finestructure values (or wind-induced mixed layers) observed in the open expanses of the Banda Sea and between Australia and Indonesia in the vicinity of 130°E, 9°S. For the 100 to 300 m layer (Figure 12b), below the maximum impact of the monsoon winds, several deep strait locations are most notable with significantly high finestructure values even where the ocean bottom is deeper than 760 m: Alor Strait (near 124°E, 8°S m), Ombai Strait (near 125°E, 8°S), and the broad Lifamatola Strait (near 126°E, 2°S). Conversely, locations more distant from the coasts generally have much lower finestructure values. For deeper layers, such as 500 to 700 m, the deep straits are exclusively highlighted with the highest finestructure values only in the Alor, Ombai, and Lifamatola Straits, and the narrow passage near 117°E, 6°S (Figure 12c).

[18] The two example "snapshot" finestructure profiles shown in Figure 9 are consistent with these spatially averaged finestructure results (Figure 12b, to get below much of the monsoon signal) with correspondingly high finestructure values in the Ombai Strait region and low finestructure values in much of the Flores Sea region.

5.2. Transect Sections

[19] The results can be shown along five XBT transect sections capturing the three variations in the west–east shipping lanes and the two variations in the north–south shipping lanes. In this equatorial region, the temperature sections [see *Wijffels and Meyers*, 2004] have relatively small geographic variability, but large vertical temperature gradients with the warmest temperatures (on order of 30°C) near the surface decreasing in typical fashion to colder temperatures (on order of 10°C) near 300 m. Sections of the finestructure (Figures 13 and 14) show considerable geographic and depth variability and reveal the vertical details missing in the map view. The most profound features of the sections are the top-to-bottom enhancement in finestructure values for the Lifamatola (Figure 13; 126°E, 2°S), Alor (not shown; 124°E, 8°S), and Ombai (Figure 13;

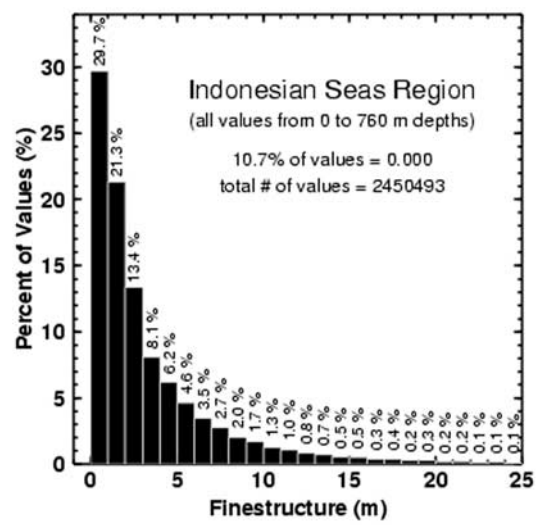

Figure 11. The histogram of all the finestructure values in the Indonesian Seas region from the sea surface down to 760-m depths. This plot enables the extreme values of the finestructure values to be assessed, whereas the previous plot (Figure 10) best characterizes the central values of the data distribution. This histogram distribution reveals that most of the finestructure values are less than 2 m, with 10.7% of the values equaling zero indicating a smoothly varying temperature profile. The percentage of finestructure values between 0 and 5 m is 78.7% of the values. The larger finestructure values, although increasingly proportionally fewer in number, should not be necessarily considered "outliers" but as possible indicators of infrequent but energetic phenomena/events.

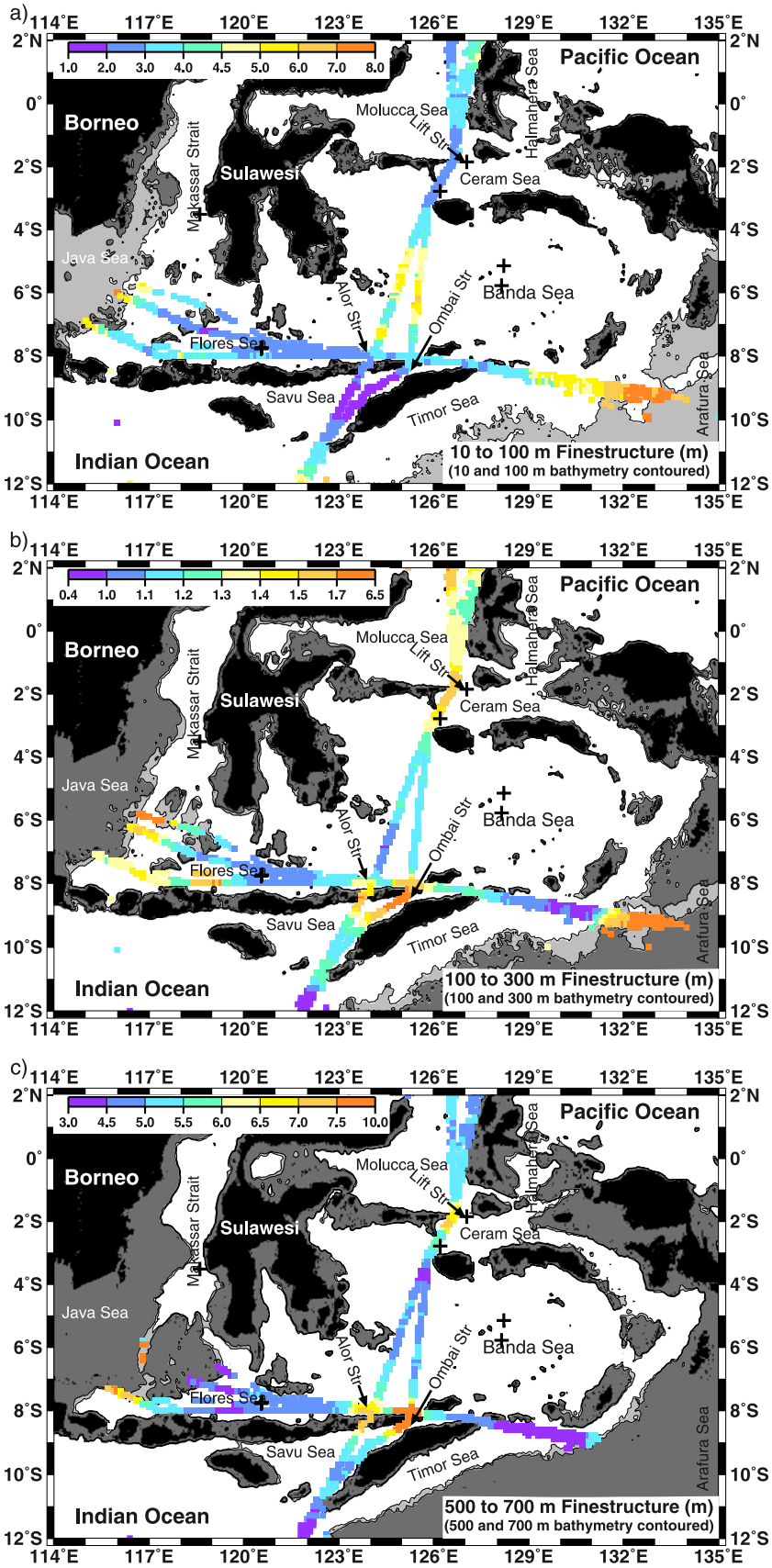
a)
1.0 2.0 3.0 4.0 4.5 5.0 6.0 7.0 8.0
Pacific Ocean
Borneo
Molucca Sea
Lift Str
Halmahera Sea
Makassar Strait
Sulawesi
Ceram Sea
Java Sea
Alor Str
Ombai Str
Banda Sea
Flores Sea
Savu Sea
Timor Sea
Arafura Sea
Indian Ocean
10 to 100 m Finestructure (m)
(10 and 100 m bathymetry contoured)
b)
0.4 1.0 1.1 1.2 1.3 1.4 1.5 1.7 6.5
100 to 300 m Finestructure (m)
(100 and 300 m bathymetry contoured)
c)
3.0 4.5 5.0 5.5 6.0 6.5 7.0 7.5 10.0
500 to 700 m Finestructure (m)
(500 and 700 m bathymetry contoured)
114°E 117°E 120°E 123°E 126°E 129°E 132°E 135°E
2°N 0° 2°S 4°S 6°S 8°S 10°S 12°S

Figure 12

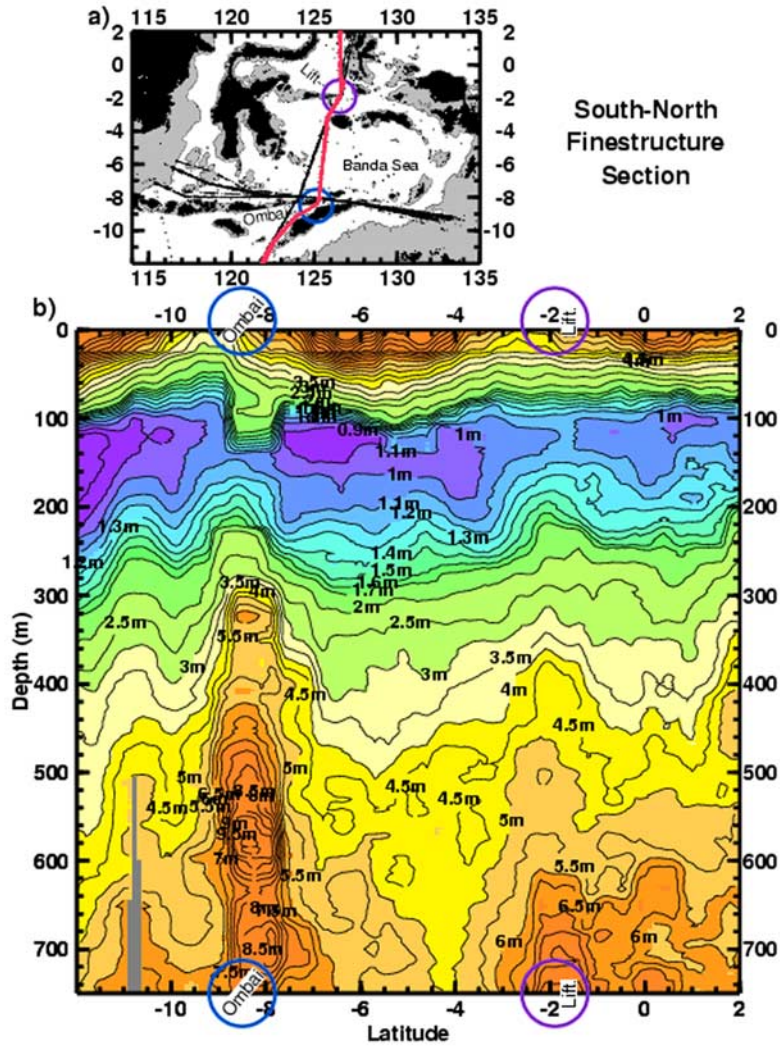

Figure 13. The north–south section of (b) finestructure through the Ombai Strait (near 125°E, 8°S) and the Lifamatola Strait (near 126°E, 2°S). The contour units are meters. The (a) map of the XBT station locations with the stations used in this section highlighted. The map bathymetry is grey shaded and contoured for 300-m depths and is white for depths greater than 300 m.

125°E, 8°S) Straits contrasted by low values in the mid-thermocline of the midbasins (dark blues). Particularly high enhancement in finestructure values are also observed laterally outward from the shallow Northwest Australian Shelf (east of 129°E and shallower than 300 m), but they are best observed in an anomaly sections which are not included here.

5.3. Association With Bathymetry

[20] In the Indonesian Seas region, as might be expected, the finestructure results reveal enhancement associated with proximity to topography. The finestructure results compiled as a function of distance to the nearest 100 m bathymetry, consistently reveal in the median, mean, 75%, and 87.5% statistics, the largest finestructure values within 5 km, "medium" values between 5 and 35 km, and the lowest values at distances greater than 35 km (Figure 15). The 100 m bathymetry is a good approximation for the shelf-slope break, which is associated with the generation of internal tides/waves. The depths between 400 and 760 m are shown in order to focus on the bathymetry dependence of the deeper off-shelf regions. The XBT observations that are farthest away from 100 m bathymetry, 120 km and greater distance, are located in the Banda Sea, at 125.5°E and 4.5°S, and at the extreme southern end of the study region, 122.0°E and 12.0°S. Consistent with finestructure enhancement near

Figure 12. A map of the finestructure averaged for (a) 10–100-m, (b) 100–300-m, and (c) 500–700-m depths along the XBT transects. The data are binned in 0.1° squares and smoothed heavily by a 3° by 3° filter. At least 2 points are required for each 0.1° square, although along the main XBT transects this criterion is far exceeded (see Figure 2). Land is black, and the bathymetry is contoured as indicated in each figure. The locations of the eight CTD yo-yo stations are indicated by crosses.

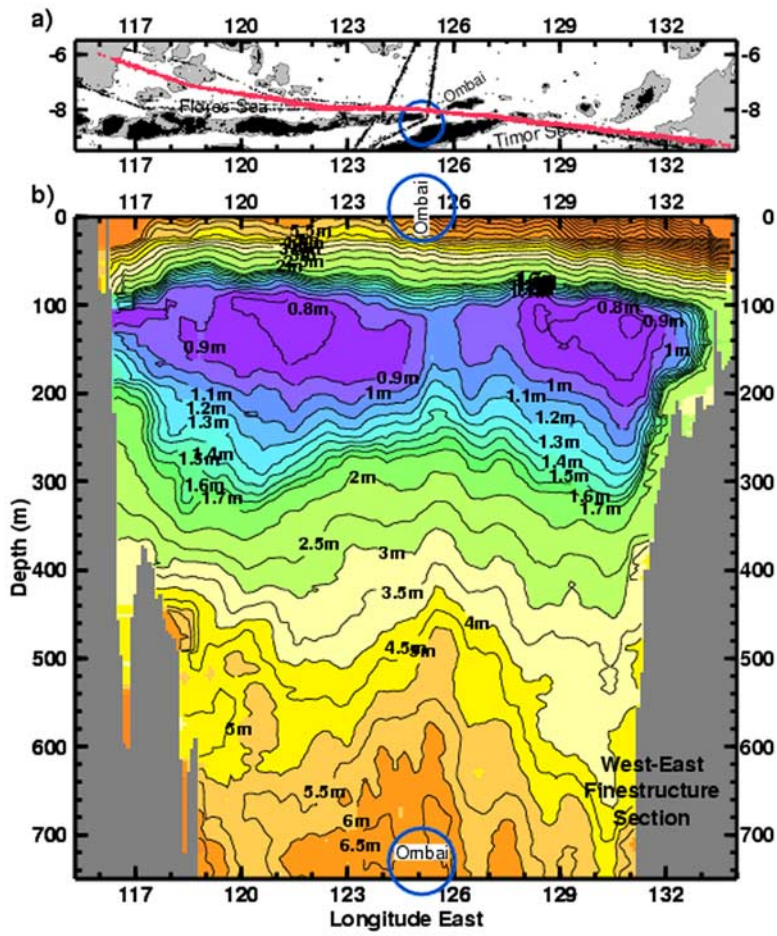

Figure 14. The west–east section of (b) finestructure through the central Flores Sea (120°E, 7°S) and the Ombai (near 125°E, 8°S) and Wetar Straits (near 126°E, 8°S). The contour units are meters. The (a) map of the XBT station locations with the stations used in this section highlighted. The map bathymetry is grey shaded and contoured for 300-m depths and is white for depths greater than 300 m.

topography, large temperature variability is observed near shelf-slope breaks in the Indonesian Seas [*Wijffels and Meyers*, 2004] and intensive ocean internal waves are observed emanating outward from straits [*Susanto et al.*, 2005].

[21] Two histograms comparing the within 5 km results to the 35 km and more distant results reveal the now-familiar histogram shape with most values tending toward zero indicative of a smoothly varying temperature profile (Figure 16, the results for 500- to 600-m depths). However, the results nearest to bathymetry are consistently proportionately-dominated by large values (black line) in comparison to the results distant from bathymetry that are consistently proportionately-dominated by small values (solid grey). This histogram comparison (Figure 16) highlights the differences at the finestructure extremes (e.g., from 10 to 40 m) that are essentially not represented by the box and whiskers plot that best illuminates central values of the distributions (Figure 15).

5.4. Monsoon Time Scales

[22] In order to further characterize the temperature finestructure in the Indonesian Seas region, the time variability is examined, capitalizing on the lengthy 21-year XBT time series. The monthly means of temperature, vertical temperature gradient (for completeness), and finestructure are determined to first examine the influence of the monsoons.

[23] In the uppermost 0 to 100 m shallow layer, the resulting annual mean time series reveal remarkably similar temperature (Figure 17a, solid line, spread of 1.2°C) and finestructure (Figure 17a, dashed line, spread of 5.4 m) curves, with the most-striking features being the highest finestructure in July and the coldest temperatures in August. The maximum correlation between temperature and finestructure is −0.93 when temperature is lagged one month (i.e., temperature changes follow 1 month later) and is easily identified by eye on the plot from July to December (note that in January to April there does not seem to be any lag). The finestructure curve itself is suggestive of direct wind forcing as it mimics the general wind magnitude in the region, in particular in the Banda Sea, with highest finestructure (7.0 m) and strongest winds during the Southeast Monsoon (June, July, and August) and half as strong finestructure (3.5 m) and about half as strong winds during the Northwest Monsoon (December, January, and February, maximum in February). Studies using satellite wind data in the Indonesian Seas region are consistent with these finestructure results and describe the effect of the wind in much

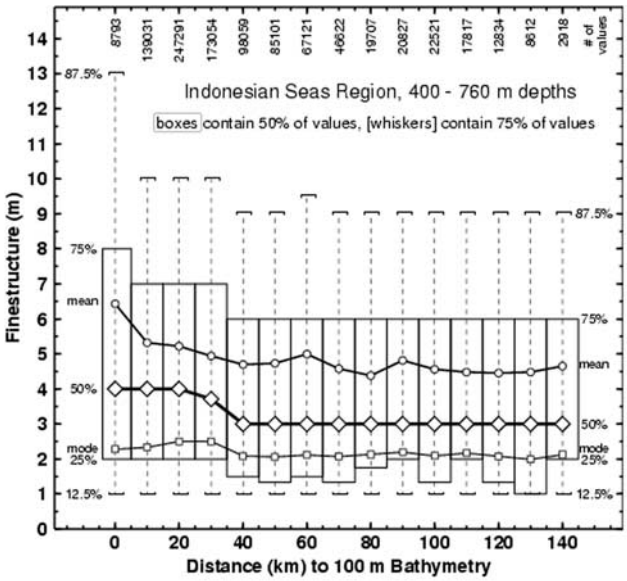

Figure 15. The (circles) mean finestructure as a function of distance from the nearest 100 m bathymetry, and the (squares) mode, (diamond) median, (boxes) middle 50% of values, and (whiskers) middle 75% of values to indicate the central spread of the finestructure values. The number of observations per distance interval is indicated along the top of the plot. The data include the entire Indonesian Seas region (114°W, 135°W, 12°S, 2°N), and for depths between 400 and 760 m in order to focus on the bathymetry dependence of the deeper off-shelf regions. Note that the finestructure values are largest, closest to the 100-m bathymetry, especially within 5 km of the 100-m bathymetry, and that the enhancement with nearness to bathymetry is observed out to 35-km distance.

greater detail [*Sprintall and Liu*, 2005; *Gordon and Susanto*, 2001]. The Southeast Monsoon finestructure is a 63% enhancement relative to the low-wind intermonsoon months of September, October, and November.

[24] Consistent with direct forcing by the wind at the sea surface, the average vertical profile of finestructure for the windy Southeast Monsoon time period (Figure 18c, "JJA" dashed line) is the most striking feature with maximum displacement (15 m) at the sea surface and enhanced values confined to the upper 100 m of the profile. As the signal is so clearly surface dominated, it is probably indicative of wind-induced turbulence and mixing that act to cool the upper layer temperature by mixing deeper and cooler thermocline water up into the surface layer. The geographic variability in the monsoon signal is also revealed in the annual average finestructure map-view for 10- to 100-m depths (Figure 12a) where the expansive regions in the middle of the Banda Sea and between Australia and Indonesia, which potentially have the longest fetch during the strongest winds of the Southeast Monsoon, have the highest finestructure values. Additional atmospheric-derived forcing can modulate temperature: (1) As most of the region is south of the equator, solar heating is maximum during December (contributing to warmer temperatures during the Northwest Monsoon) and minimum during June (contributing to cooler temperatures during the Southeast Monsoon). (2) The rainy season is during the Northwest Monsoon; the dry season is during the Southeast Monsoon when very strong and dry winds blow off of Australia contributing to cooling of the ocean by evaporation in June, July, and August. (3) In the Banda Sea downwelling occurs in January, February, and March with the maximum in February (associated with warmer upper layer temperatures) and upwelling (associated with cooler upper layer temperatures) during the rest of the year with maximum in May and June [*Gordon and Susanto*, 2001] overlapping with the Southeast Monsoon. Also maximum Indonesian Throughflow during August to September may contribute to higher finestructure values.

[25] In summary, during June, July, and August of the Southeast Monsoon, all the above mentioned factors, upwelling, increased finestructure (i.e., possibly mixing), reduced solar heating, increased evaporation, can contribute toward a cooler upper ocean, corresponding to the coldest mean-annual temperatures observed in the upper layer. Whereas during December, January, and February of the Northwest Monsoon, only the secondary maximum in finestructure (probably wind-induced) can contribute to cooling the upper layer ocean (all the others are warming effects) corresponding to the secondary minimum in temperature observed in the upper layer. These different combinations of factors may explain the apparent 0-month lag in the secondary temperature minimum in February, when only wind-induced finestructure is associated with cooling, a

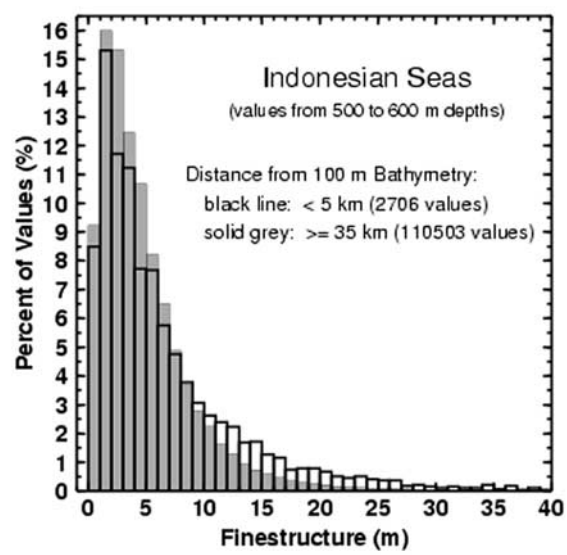

Figure 16. The histogram of the finestructure observations near (<5 km, black line) the 100-m bathymetry compared to those far (>=35 km, solid grey) from the 100-m bathymetry, for the Indonesian Seas region (114°W, 135°W, 12°S, 2°N) between 500- and 600-m depths. This plot enables the extreme values of the finestructure values to be assessed, whereas the previous plot (Figure 15) best characterizes the central values of the data distribution. Note the contrast in distribution of values for near distances versus far distances: a higher proportion of small (<9 m) finestructure values consistently dominate at far distances, whereas a higher proportion of large (> = 9 m) finestructure values usually dominate at near distances.

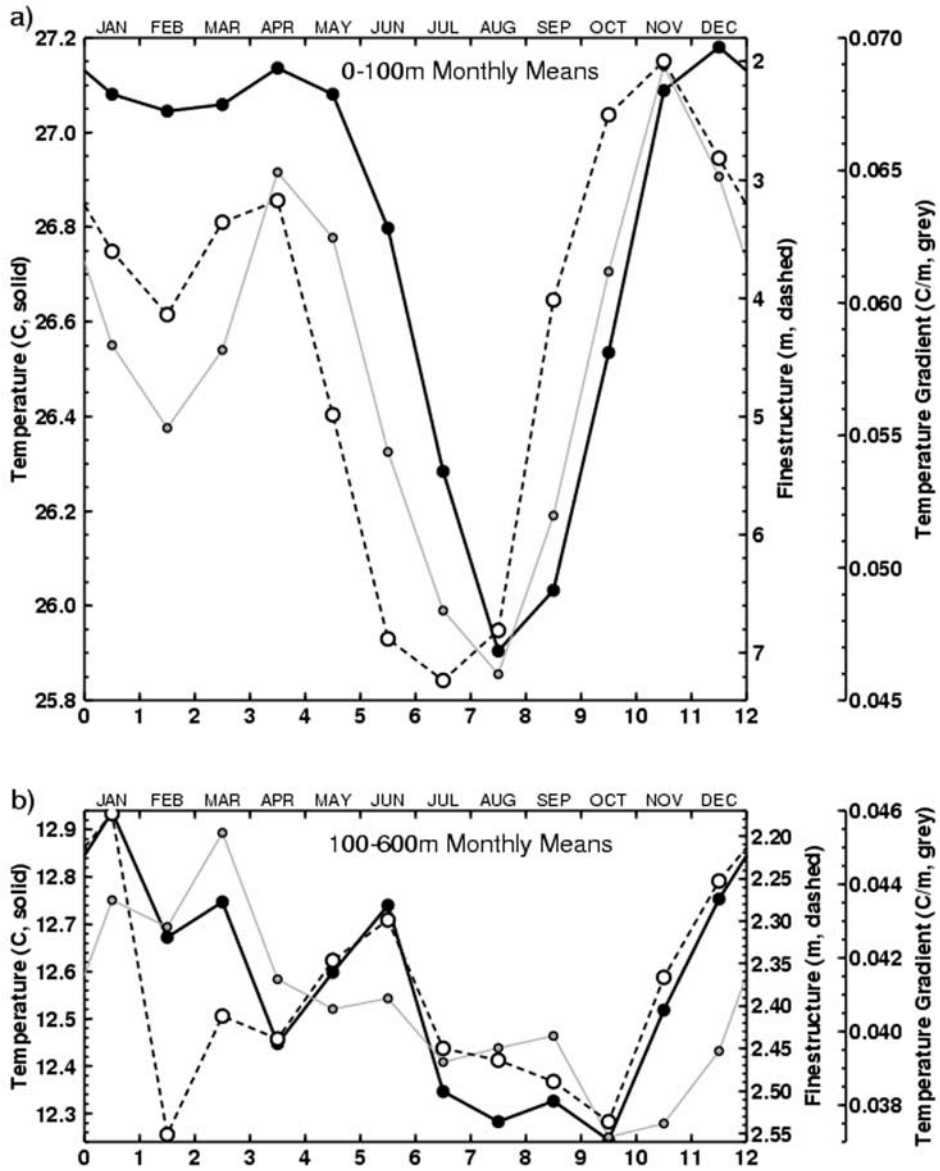

Figure 17. Monthly (solid line) mean temperature, (dashed line) finestructure and (grey line) vertical temperature gradient for the (a) 0 to 100 m layer and (b) 100 to 600 m layer in the 114°E to 135°E and 12°S to 2°N region. Note that the finestructure time series is inverted to enable easier comparison to the temperature and temperature gradient time series.

mechanism acting relatively quickly throughout the upper layer, albeit with lessening influence with depth. In contrast, the obvious 1-month lag in minimum temperature in August when cooling induced by reduced solar heating and increased evaporation acts directly only at the sea surface and takes time to be mixed downward into the ocean, then combining with the faster cooling effects attributable to the finestructure.

[26] In the 100 to 600 m deeper layer (Figure 17b), the resulting annual mean time series reveal somewhat similar temperature (range of 0.7°C) and finestructure (range of 0.3 m) curves, except that the highest finestructure values are clearly in October, three months later than in the surface layer. The maximum correlation between temperature and finestructure is −0.78 at zero lag, consistent with a cooling mechanism directly acting throughout the thermocline and relative isolation from sea surface solar heating and evaporation effects. However, the annual mean signals are much reduced in the deeper layer than in the shallow layer, such that in the finestructure full-depth profile the monsoonal variability is not obvious by eye below 100 m (Figure 18c).

5.5. Interannual Time Scales

[27] Previously the XBT data have been used to show the ENSO temperature variability in the thermocline of the Indonesian Seas [*Bray et al.*, 1996], which has been observed in other temperature data sets as well [*Sprintall et al.*, 2003; *Ffield et al.*, 2000]. Here this time variability is easily observed by spatially averaging all the temperature profiles within the Indonesian Seas region and constructing

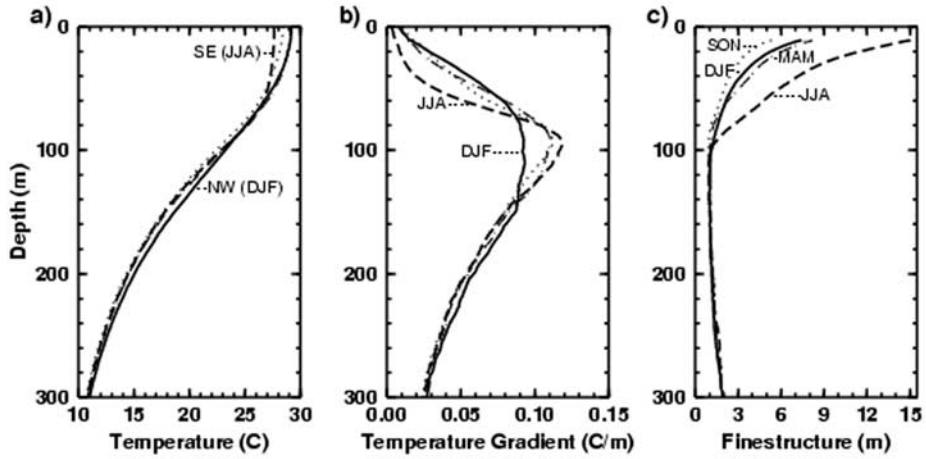

Figure 18. (a) Mean temperature, (b) temperature gradient, and (c) finestructure profiles for the 114°E to 135°E and 12°S to 2°N region and for four monsoon time periods. The northwest monsoon (NW) time period includes December, January, and February; the NW to SE transition time period includes March, April, and May; the southeast monsoon (SE) time period includes June, July, and August; and the SE to NW transition time period includes September, October, and November. Data prior to 1988 are excluded.

a single time-depth section of temperature (Figure 19). Ocean temperatures throughout the Indonesian Seas (and the western Pacific Ocean) are cooler (a shallower thermocline) during El Niño and warmer (a deeper thermocline) during La Niña throughout the water column, with a maximum signal around 150-m depth. At 150 m, during the El Niño of 1997–1998, the temperatures are ~1.5°C cooler than usual when the thermocline shallows, versus during the La Niña of 1988–1989, the temperatures are ~1.5°C warmer than usual when the thermocline deepens. (The Figure 19 section terminates at 300-m depth, as temperature variability at deeper depths cannot be observed by eye at these plot scales.) These time series section results can also be observed in two averaged profiles for the Indonesian Seas region by partitioning all the data into either an El Niño or a La Niña time period (based on the Nino3 index without any lag); the El Niño time period profile (Figure 20, solid line) is cooler throughout the thermocline, from the surface down to ~300-m depths, than the La Niña time period profile (Figure 20, dashed line).

[28] The time variability in finestructure is also shown by spatially averaging all the finestructure profiles in the Indonesian Seas region and constructing a single time-depth section of finestructure (Figure 21). The finestructure is modulated by ENSO as the temperature is, but surprising the modulation of the finestructure in the shallow layer is opposite to that in the deeper layer: the shallow layer finestructure values are smaller (larger) during El Niño (La Niña), but in the deeper layer they are larger (smaller) during El Niño (La Niña). This can also be observed by constructing two averaged profiles using all the Indonesian Seas region data separated by ENSO period (defined by Nino 3 without any lag); the finestructure is reduced from the surface to 100-m depths in El Niño profile, but the finestructure is elevated from 100- to 600-m depths in El Niño profile (Figure 20c, solid line) and the La Niña is the opposite pattern (Figure 20, dashed line). Between 100- and 600-m depth, the El Niño finestructure is a 10% enhancement over the La Niña finestructure (with zero lag), and the enhancement increases slightly to 13% if the finestructure values are all lagged 6 months when defining the ENSO time periods.

[29] The average temperature profiles (Figure 20a) show the shallower Indonesian thermocline during El Niño (and therefore colder at each depth) versus the deeper La Niña thermocline (and therefore warmer at each depth). In addition, the corresponding vertical temperature gradient profiles reveal stronger vertical gradients in the shallow, 0 to 100 m, layer during El Niño than during La Niña, but weaker vertical gradients in the deeper, 100 to 500 m, layer during El Niño than during La Niña (Figure 20b). Weaker (stronger) vertical temperature gradients imply decreased (increased) water column stability and when perturbed increased (decreased) vertical displacements/modifications within the water column. Therefore the ENSO differences in vertical temperature gradients may be responsible for the observed ENSO modulation of the finestructure. For example, when the temperature gradients imply decreased (increased) water column stability in the 100 to 500 m layer during El Niño (La Niña), the finestructure is in fact higher (lower) as is expected with this hypothesis (Figure 20c). In contrast, if this were a quiescent internal wave region, then large-scale thermocline stability changes due to basin-wide processes might not necessarily impact the local finestructure. However, in the Indonesian Seas, it seems as if the internal wave activity, as well as any necessary "threshold" background conditions, are sufficient enough, such that a change in the stability of the water column leads to measurable finestructure changes. In fact, the El Niño finestructure seems to be more chaotic (Figures 20c and 21) then would be simply predicted by the observed El Niño temperature gradient changes (Figures 19 and 20b), suggesting that the interaction of multiple factors should be considered in future studies.

[30] The results can be considered in further detail by assessing the combined monsoon and ENSO variability (not shown). As mentioned above, in the upper 100-m depth the finestructure is highest during the windy Southeast Monsoon.

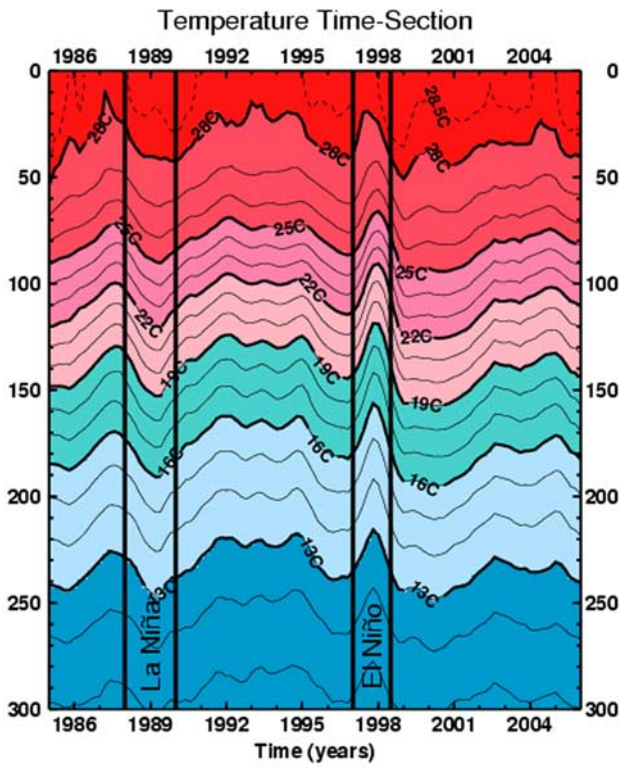

Figure 19. The temperature time-depth section averaged over the 114°E to 135°E and 12°S to 2°N Indonesian Seas region. ENSO variability is easily observed from the ocean surface down to the bottom of the XBT profiles ~760 m; this section only shows the upper 300 m of the water column in order to expand the midthermocline levels which have the largest ENSO signal at ~150 m. Ocean temperatures throughout the Indonesian Seas (and the western Pacific Ocean) are cooler during El Niño and warmer during La Niña; for example, in this section at 150 m they attain temperatures ~1.5°C cooler than usual during the El Niño of 1997–1998 when the thermocline shallows and temperatures ~1.25°C warmer than usual during the La Niña of 1988–1989 when the thermocline deepens. The data are smoothed by a 20-m vertical filter and then a 1-year horizontal filter.

However, it is during the Southeast Monsoon La Niña months that have the highest finestructure (8.0 m) albeit delayed until August, whereas during the Southeast Monsoon El Niño months the finestructure is relatively lower (6.4 m) and is observed earlier in June–July. This is consistent with winds generally being reduced during El Niño time periods in the Indonesian Seas region (associated with low rainfall and drought). From 100- to 600-m depth the finestructure is highest (3.8 m) during March–April El Niño months, whereas the remainder of the time periods do not have a definitive signal and have overall lower finestructure values (averaging around 2.6 m); it is not obvious as to the origin of this signal.

6. Discussion

[31] The results of the finestructure analysis can be used as a qualitative background framework in which to understand snapshot high-resolution dedicated measurements, even when the measurements do not fall directly along the XBT ship of opportunity shipping lanes. In the Banda Sea, the microstructure measurements from 22 October to 7 November 1998 [*Alford and Gregg*, 1999] culminated in a cruise-mean diapycnal diffusivity of $9.2 \pm 0.55 \times 10^{-6}$ m^{2}s^{-1} between 20- and 300-m depths, a value similar to "open ocean" estimates. Due to the location and timing of the microstructure experiment, this measured value may be lower than the average diffusivity for the Indonesian Seas region. The microstructure measurements were obtained at 128°E, 6.5°S in the central Banda Sea, relatively far, 90 km, from the nearest 100 m topography to the southeast, and not surrounded by topography, implying reduced topographic influence. In addition, the microstructure measurements reveal three cycles of discrete energetic mixing by a near-inertial wave during the 14-day experiment. However, using satellite wind data, a model of wind-generated near-inertial wave mixing suggests that this mixing by near-inertial waves could be up to three orders of magnitude higher during the height of the monsoons [*Alford and Gregg*, 2001, Figure 17]. It is reasonable to consider the possibility that variability in finestructure may ultimately be associated with a corresponding variability in vertical mixing. The microstructure measurements are consistent with the framework developed from the finestructure results, as the microstructure experiment time period can be identified as the low-wind monsoon transition months of October and November with the seasonally lowest finestructure in the upper 100 m (Figure 17, dashed line, and Figure 18c), and to a lesser extent, as the onset of La Niña in late 1998 with slightly reduced averaged surface to 300-m depths finestructure (Figure 20c), as well as distant from topography with reduced finestructure (Figure 15, 90 km distance). In this way, it is reasonable to consider the possibility that the microstructure measurements may be a lower bound for diapycnal diffusivity in the Indonesian Seas region as the authors of the microstructure study already did using the satellite wind data [*Alford and Gregg*, 2001]. However, with the finestructure results, the inference is based on data obtained from within the oceanic water column, whereas in the microstructure study the inference is based on data obtained from the atmosphere.

[32] Tidal modeling studies in the Indonesian Seas region predict large and complex tides [*Ray et al.*, 2005] that are associated with isotherm variability and vertical mixing. The large-scale tides ultimately dissipate at small scales, and the finestructure identified in this paper lies intermediate to those scales. In a recent study designed to quantify the overall magnitude of the M_2 baroclinic tides in the Indonesian Seas region [*Robertson and Ffield*, 2005], a striking feature is the enhancement of the M_2 baroclinic (depth-varying and produced by interaction with topography) tidal currents over the M_2 barotropic (uniform with depth) tidal currents. In the Banda Sea, the M_2 barotropic tidal currents are only between 0 and 5 cm s^{-1}, whereas the maximum M_2 baroclinic tidal currents are much higher between 5 and 40 cm s^{-1} [*Robertson and Ffield*, 2005, Figures 3b and 3c]. The same relationship holds for the rest of the non-shelf Indonesian Seas region; for example in the Lifamatola Strait, the M_2 barotropic tidal currents are between 10 and 20 cm s^{-1} with high values only at the side-walls of the

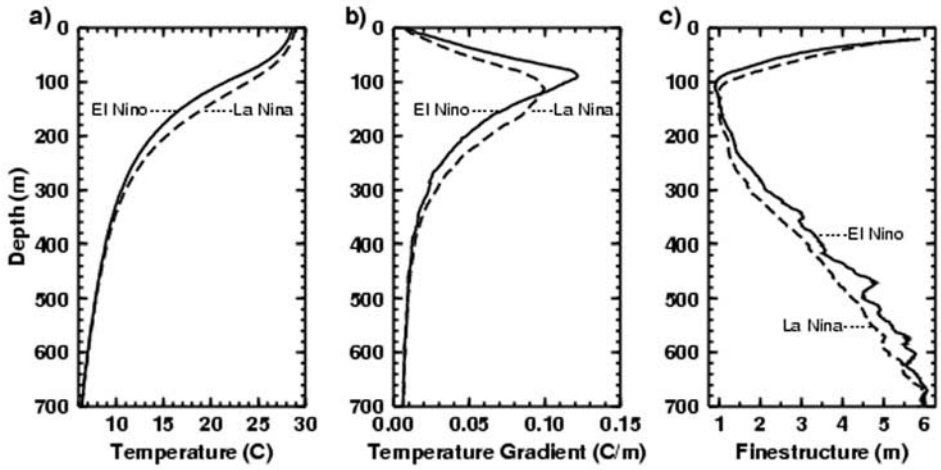

Figure 20. (a) Mean temperature, (b) temperature gradient, and (c) finestructure profiles for the 114°E to 135°E and 12°S to 2°N region and the El Niño and La Niña time periods. During El Niño (solid line, NINO3 index >0.5) the temperature profile is higher in the region relative to La Niña (dashed line, NINO3 index <0.5). The corresponding vertical temperature gradients during El Niño are stronger from 0 to 100 m and weaker below 100 m relative to La Niña. Data prior to 1988 are excluded.

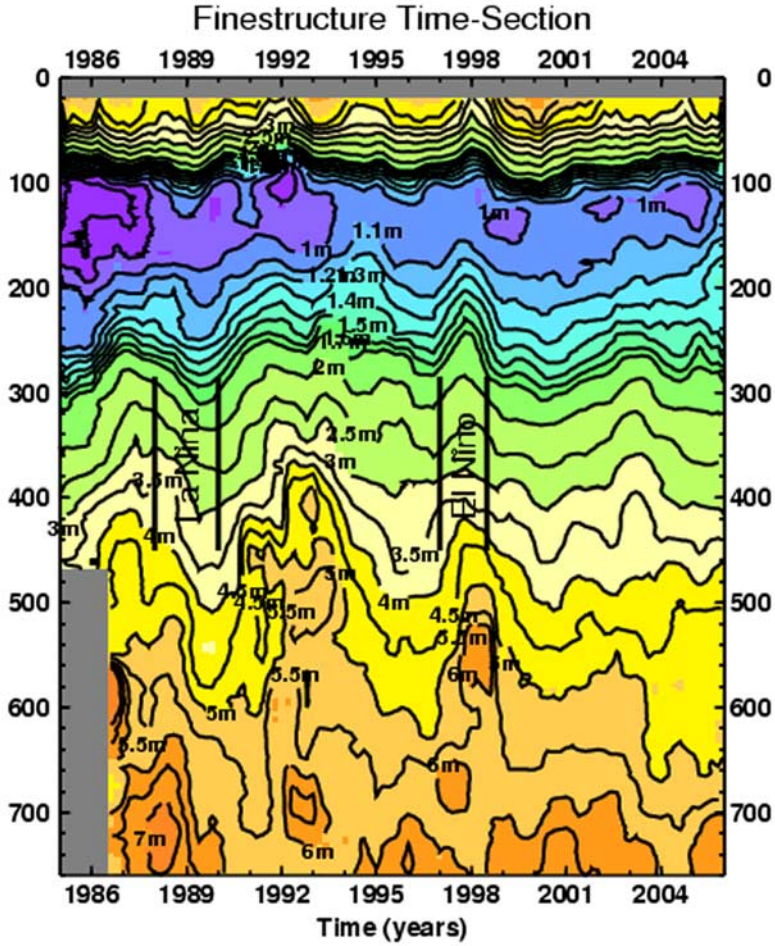

Figure 21. The finestructure time-depth section averaged over the 114°E to 135°E and 12°S to 2°N Indonesian Seas region. The data are smoothed by a 50-m vertical filter and then a 1-year horizontal filter.

strait, whereas the maximum M_2 baroclinic tidal currents are higher than 50 cm s^{-1} for most of the Lifamatola Strait region and extend outward in all directions. In general, the spatial variability in the predicted baroclinic tidal currents is remarkably consistent with the spatial variability observed in the finestructure at depths below the main influence of the monsoons (Figures 12b and 12c). This is not unexpected, as the baroclinic tides are generated at topography and the finestructure enhancement with topography is already noted (Figure 15). The around monthly resolution of the XBT data coupled with the significant spatial, depth, seasonal, and interannual thermocline stratification variability precludes any definitive analysis at tidal time-scales in this large-scale averaged treatment of the XBT data. In the Indonesian Seas region, all locations are potentially influenced by internal tides generated from multiple sites. With the monsoonal and interannual changing thermocline stratification, it is likely that the time, location, and magnitude of the internal tide features have a monsoonal and interannual variability as well.

[33] This study quantifies the finestructure throughout the Indonesian Seas, but bona fide vertical mixing studies are needed in order to answer important questions. The thermocline in the tropical Indonesian Seas region is highly stratified, and coupled with vertical mixing, large fluxes of heat and buoyancy are implied from the ocean-atmosphere boundary downward deep into the water column. To accurately predict climate change requires quantifying this vertical mixing and its temporal and spatial variability, because these fluxes help regulate ocean heat storage and thermohaline circulation. In addition, the modulation of the sea surface temperature by oceanic vertical mixing can directly impact the atmosphere at short time scales through ocean-atmosphere interaction [*Qu et al.*, 2005]. As droughts are associated with the anomalously cool sea surface temperatures during El Niño in the Indonesian Seas region, this is also an important relationship to quantify.

[34] The finestructure analysis of 21-years of XBT data reveals significant temporal and horizontal and vertical variability throughout the Indonesian Seas region. The results should only be generally interpreted, as the analysis treats the region as an oceanographically similar entity when in fact different water masses, dynamics, north versus south of the equator, and Pacific versus Indian Ocean forces may uniquely define the variability at a single location and time. For example, the volume transport of the Indonesian Throughflow is highest (lowest) during La Niña (El Niño) [*Meyers*, 1996], with a varying depth distribution [*Susanto and Gordon*, 2005], and these changes can modulate the current shear and vertical mixing. Also there is additional salty South Pacific water entering the eastern Indonesian Seas during the Northwest Monsoon with associated horizontal intrusions [*Ilahude and Gordon*, 1996] that will change the stability of the water column and internal tide generation characteristics.

7. Conclusions

[35] Throughout the Indonesian Seas region, the smaller-scale vertical temperature variability, or finestructure, is observed to vary considerably as a function of location, depth, season, and year. Twelve-hour CTD yo-yo stations, scattered throughout the Indonesian Seas, provide a glimpse of the variability with a variety of smaller-scale vertical temperature and salinity features in the profiles, and different internal wave heaving signatures. In order to qualitatively characterize the spatial and temporal variability in finestructure throughout the Indonesian Seas region, 21-years of XBT temperature profiles are analyzed. From the results, a consistent spatial variability emerges, with clear enhancement in finestructure associated with straits, shallow shelves, and proximity to the shelf-slope boundary. In the upper 100 m of the water column, monsoonal variability dominates, with highest finestructure values during the windy June, July, and August Southeast Monsoon time period when the upper thermocline is less stratified, especially during La Niña years, and lowest finestructure values during the low-wind September, October, November intermonsoon time period when the upper thermocline is more stratified, especially during El Niño years. At deeper levels in the water column interannual variability dominates, with highest finestructure values during El Niño between 100- and 600-m depths, when the lower thermocline is less stratified (in contrast to the upper thermocline), and lowest finestructure values during La Niña between 100- and 600-m depths, when the lower thermocline is more stratified (in contrast to the upper thermocline).

[36] **Acknowledgments.** This project was supported by the Office of Naval Research, NOOO14-03-1-0423. The XBT data used in the paper were collected under the Joint CSIRO and Bureau of Meteorology's Australian Facility for Ocean Observations. We thank all the crews and shipping companies that have volunteered to collect these data.

References

Alford, M. H., and M. C. Gregg (1999), Diapycnal mixing in the Banda Sea: Results of the First microstructure measurements in the Indonesian throughflow, *Geophys. Res. Lett.*, *26*, 741–2744.

Alford, M. H., and M. C. Gregg (2001), Near-inertial mixing: Modulation of shear, strain and microstructure at low latitude, *J. Geophys. Res.*, *106*, 16,947–16,968.

Bray, N. A., et al. (1996), Large-scale sea level, thermocline, and wind variations in the Indonesian throughflow region, *J. Geophys. Res.*, *101*, 12,421–12,432.

Desaubies, Y., and M. C. Gregg (1981), Reversible and Irreversible Finestructure, *J. Phys. Oceanogr.*, *11*, 541–556.

Dillon, T. M. (1982), Vertical overturns: A comparison of Thorpe and Ozmidov length scales, *J. Geophys. Res.*, *87*, 9601–9613.

Ffield, A., and A. L. Gordon (1992), Vertical mixing in the Indonesian thermocline, *J. Phys. Oceanogr.*, *22*, 184–195.

Ffield, A., and A. L. Gordon (1996), Tidal mixing signatures in the Indonesian Seas, *J. Phys. Oceanogr.*, *26*, 1924–1937.

Ffield, A., et al. (2000), Temperature variability within Makassar Strait, *Geophys. Res. Lett.*, *27*, 237–240.

Finnigan, T. D., et al. (2002), Observations of enhanced diapycnal mixing near the Hawaiian ridge, *J. Phys. Oceanogr.*, *32*, 2988–3002.

Gordon, A. L. (2005), Oceanography of the Indonesian Seas and their throughflow, *Oceanography*, *18*, 14–27.

Gordon, A. L., and R. D. Susanto (2001), Banda Sea surface-layer divergence, *Ocean Dyn.*, *52*, 2–10.

Hatayama, T. (2004), Transformation of the Indonesian throughflow water by vertical mixing and its relation to tidally generated internal waves, *J. Oceanogr.*, *60*, 569–585.

Hatayama, T., et al. (1996), Tidal currents in the Indonesian seas and their effect on transport and mixing, *J. Geophys. Res.*, *101*, 12,353–12,373.

Hautala, S. L., et al. (1996), The distribution and mixing of Pacific water masses in the Indonesian Seas, *J. Geophys. Res.*, *101*, 12,375–12,389.

Ilahude, A. G., and A. L. Gordon (1996), Thermocline stratification within the Indonesian seas, *J. Geophys. Res.*, *101*, 12,401–12,409.

Kunze, E., et al. (2006), Global abyssal mixing inferred from lowered ADCP shear and CTD strain profiles, *J. Phys. Oceanogr.*, *36*, 1553–1576.

Meyers, G. (1996), Variation of Indonesian throughflow and the El Niño-Southern Oscillation, *J. Geophys. Res.*, *101*, 12,255–12,263.

Molcard, R. M., et al. (1996), The Indo-Pacific throughflow in the Timor Passage, *J. Geophys. Res.*, *101*, 12,411–12,420.
Molcard, R. M., et al. (2001), The throughflow within Ombai Strait, *Deep Sea Res.*, *48*, 1237–1253.
Murray, S. P., and D. Arief (1988), Throughflow into the Indian Ocean through the Lombok Strait, January 1985–Janary 1986, *Nature*, *333*, 444–447.
Murtugudde, R. A., et al. (1998), Seasonal-to-interannual effects of the Indonesian throughflow on the tropical Indo-Pacific Basin, *J. Geophys. Res.*, *103*, 21,425–21,441.
Polzin, K. L., et al. (1995), Finescale parameterizations of turbulent dissipation, *J. Phys. Oceanogr.*, *25*, 306–328.
Qu, T., et al. (2005), Sea surface temperature and its variability in the Indonesian region, *Oceanography*, *18*, 50–61.
Ray, R. D., et al. (2005), A brief overview of tides in the Indonesian Seas, *Oceanography*, *18*, 74–79.
Robertson, R., and A. Ffield (2005), M_2 baroclinic rides in the Indonesian Seas, *Oceanography*, *18*, 62–73.
Schiller, A., et al. (1998), Seasonal near-surface dynamics and thermodynamics of the Indian Ocean and Indonesian throughflow in a global ocean general circulation model, *J. Phys. Oceanogr.*, *28*, 2288–2312.
Sprintall, J., and W. T. Liu (2005), Ekman mass and heat transport in the Indonesian Seas, *Oceanography*, *18*, 88–97.
Sprintall, J., et al. (2003), Temperature and salinity variability in the exit passages of the Indonesian throughflow, *Deep Sea Res, Part II*, *50*, 2183–2204.
Susanto, R. D., and A. L. Gordon (2005), Velocity and transport of the Makassar Strait throughflow, *J. Geophys. Res.*, *110*, C01005, doi:10.1029/2004JC002425.
Susanto, R. D., et al. (2005), Ocean internal waves observed in the Lombok Strait, *Oceanography*, *18*, 80–87.
van Aken, H. M., et al. (1988), Physical aspects of the flushing of the East Indonesian basins, *Neth. J. Sea Res.*, *22*, 315–339.
Wijesekera, H., and T. Dillon (1991), Internal waves and mixing in the upper Equatorial Pacific Ocean, *J. Geophys. Res.*, *96*, 7115–7125.
Wijffels, S., and G. Meyers (2004), An intersection of oceanic waveguides: Variability in the Indonesian throughflow region, *J. Phys. Oceanogr.*, *34*, 1232–1253.

A. Ffield, Earth and Space Research, 290 Clausland Mountain Road, Upper Grandview, NY 10960-4113, USA. (ffield@esr.org)
R. Robertson, School of Physical, Environmental, and Mathematical Sciences, Australian Defence Force Academy, University of New South Wales, Northatt Drive, Canberra, ACT 2617, Australia. (r.robertson@adfa.edu.au)